

Three-Dimensional Analytical Solution for Hybrid Multilayered Piezoelectric Plates

S. S. Vel

Postdoctoral Research Associate,
Mem. ASME

R. C. Batra

Clifton C. Garvin Professor,
Fellow ASME

Department of Engineering Science
and Mechanics,
Virginia Polytechnic Institute
and State University,
Blacksburg, VA 24061-0219

Analytical solutions for the static three-dimensional deformations of multilayered piezoelectric rectangular plates are obtained by using the Eshelby-Stroh formalism. The laminated plate consists of homogeneous elastic or piezoelectric laminae of arbitrary thicknesses. The equations of static, linear, piezoelectricity are exactly satisfied at every point in the body. The analytical solution is in terms of an infinite series; the continuity conditions at the interfaces and boundary conditions at the edges are used to determine the coefficients. The formulation admits different boundary conditions at the edges and is applicable to thick and thin laminated plates. Results are presented for thick piezoelectric plates with two opposite edges simply supported and the other two subjected to various boundary conditions. [S0021-8936(00)01803-1]

1 Introduction

In recent years, piezoelectric materials have been integrated with structural systems to form a class of "smart structures." The piezoelectric materials are capable of altering the structure's response through sensing, actuation and control. By integrating surface-bonded and embedded actuators into structural systems, desired localized strains may be induced by applying the appropriate voltage to the actuators.

In order to successfully incorporate piezoelectric actuators into structures, the mechanical interaction between the actuators and the base structure must be fully understood. Mechanical models were developed by Crawley and de Luis [1], Im and Atluri [2], Crawley and Anderson [3], and others for piezoelectric patches mounted to top and/or bottom surfaces of a beam. Lee [4] developed a theory for laminated plates with distributed piezoelectric layers based on the classical lamination theory. Wang and Rogers [5] applied the classical lamination theory to plates with surface-bonded or embedded piezoelectric patches. A coupled first-order shear deformation theory for multilayered piezoelectric plates was presented by Huang and Wu [6]. Mitchell and Reddy's [7] coupled higher-order theory is based on an equivalent single-layer theory for the mechanical displacements and layerwise discretization of the electric potential. Numerous finite element studies have also been conducted (e.g., see Robbins and Reddy [8], Ha et al. [9], Heyliger et al. [10], and Batra and Liang [11]).

Vlasov [12], Pagano [13,14], and Srinivas and Rao [15] obtained three-dimensional analytical solutions for simply supported, laminated anisotropic elastic plates. Their method has been extended by Ray et al. [16] and Heyliger and Brooks [17] to study the cylindrical bending of laminated piezoelectric plates. Analytical solutions for the static behavior of a homogeneous simply supported, piezoelectric rectangular plate was given by Bisegna and Maceri [18] and Lee and Jiang [19]. Heyliger [20,21] provided a three-dimensional solution for the static behavior of multilayered piezoelectric rectangular plates. All the aforementioned three-dimensional solutions are restricted to piezoelectric laminates whose edges are simply supported and electrically grounded. Such solutions are useful for validating new or im-

proved plate theories ([22]) and finite element formulations ([10,23]). However, simply supported boundary conditions are less frequently realized in practice and they do not exhibit the well-known singular effects observed near clamped or traction-free edges. The available analytical solution techniques for three-dimensional deformations are incapable of analyzing laminates with clamped or traction-free edges and/or when the edges are electrically in contact with a low-permittivity medium like air, wherein the normal component of the electrical displacement vanishes.

The Eshelby-Stroh formalism ([24–26]) provides exact solutions to the governing differential equations of anisotropic materials under generalized plane-strain deformations in terms of arbitrary analytical functions. Vel and Batra [27,28] adopted a series solution for the analytic functions to analyze the generalized plane-strain deformation of laminated elastic plates subjected to arbitrary boundary conditions, and the cylindrical bending of a laminated elastic plate with embedded or surface mounted piezoceramic patches. Recently, Vel and Batra [29] generalized the Eshelby-Stroh formalism to study the three-dimensional deformations of laminated elastic rectangular plates with arbitrary boundary conditions. Here we extend this method to multilayered piezoelectric plates subjected to arbitrary boundary conditions. The edges of each lamina may be subjected to mechanical and electrical boundary conditions different from those on the adjoining laminae. The governing differential equations are solved exactly and various constants in the resulting series solution are determined from the boundary conditions at the edges and the continuity conditions at the interfaces. This results in an infinite system of equations in infinitely many unknowns. By retaining a large number of terms in the series solution, the mechanical displacements, stresses, electric potential, and electric displacement can be computed to any desired degree of accuracy. Results are presented for thick piezoelectric plates with two edges simply supported and the other two edges subjected to arbitrary boundary conditions. These results can be used to assess the accuracy of different plate theories and finite element formulations.

2 Formulation of the Problem

We use a rectangular Cartesian coordinate system, shown in Fig. 1, to describe the infinitesimal quasi-static deformations of an N -layer piezoelectric laminated plate occupying the region $[0, L_1] \times [0, L_2] \times [0, L_3]$ in the unstressed reference configuration.

Contributed by the Applied Mechanics Division of THE AMERICAN SOCIETY OF MECHANICAL ENGINEERS for publication in the ASME JOURNAL OF APPLIED MECHANICS. Manuscript received by the ASME Applied Mechanics Division, June 2, 1999; final revision, Nov. 23, 1999. Associate Technical Editor: I. M. Daniels. Discussion on the paper should be addressed to the Technical Editor, Professor Lewis T. Wheeler, Department of Mechanical Engineering, University of Houston, Houston, TX 77204-4792, and will be accepted until four months after final publication of the paper itself in the ASME JOURNAL OF APPLIED MECHANICS.

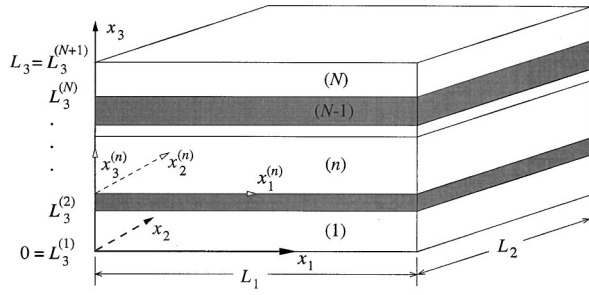


Fig. 1 An N -layer laminated piezoelectric plate

The vertical positions of the bottom and top surfaces as well as of the $N-1$ interfaces between the laminae are denoted by $L_3^{(1)}=0, L_3^{(2)}, \dots, L_3^{(n)}, \dots, L_3^{(N)}, L_3^{(N+1)}=L_3$.

The equilibrium equations and charge equations of electrostatics in the absence of body forces and free charges are

$$\sigma_{jm,m}=0, \quad D_{m,m}=0, \quad (j,m=1,2,3), \quad (1)$$

where σ_{jm} are the components of the Cauchy stress tensor and D_m the electric displacement. A comma followed by index m indicates partial differentiation with respect to the present position x_m of a material particle, and a repeated index implies summation over the range of the index.

The constitutive equations of a linear piezoelectric medium are ([30])

$$\sigma_{jm}=C_{jmqr}\varepsilon_{qr}-e_{rjm}E_r, \quad D_m=e_{mqr}\varepsilon_{qr}+\epsilon_{mr}E_r, \quad (q,r=1,2,3), \quad (2)$$

where ε_{qr} are the components of the infinitesimal strain tensor, E_r the electric field, C_{jmqr} the elasticity constants, e_{rjm} the piezoelectric moduli, and ϵ_{mnr} the electric permittivity. The infinitesimal strain tensor and electric field are related to the mechanical displacement u_q and electric potential ϕ by

$$\varepsilon_{qr}=\frac{1}{2}(u_{q,r}+u_{r,q}), \quad E_j=-\phi_{,j}. \quad (3)$$

We will interchangeably use the direct and indicial notation. The stored energy density W for a piezoelectric medium is given by ([30])

$$W=\frac{1}{2}(\sigma_{jm}\varepsilon_{jm}+D_mE_m)=\frac{1}{2}(C_{jmqr}\varepsilon_{jm}\varepsilon_{qr}+\epsilon_{mr}E_mE_r). \quad (4)$$

The symmetry of the stress and strain tensors and the existence of the stored energy function imply the following symmetry conditions:

$$C_{jmqr}=C_{mjqr}=C_{qjrm}, \quad e_{rjm}=e_{rmj}, \quad \epsilon_{mr}=\epsilon_{rm}. \quad (5)$$

In the most general case, there are 21 independent elastic constants, 18 independent piezoelectric moduli, and 6 independent dielectric permittivities. Material elasticities are assumed to yield a positive stored energy density for every nonrigid deformation and/or nonzero electric field. That is,

$$C_{jmqr}u_{,j}u_{,m}u_{,q}u_{,r}>0, \quad \epsilon_{mr}E_mE_r>0, \quad (6)$$

for every real nonzero ε_{jm} and E_m . The total stored energy U of the piezoelectric laminate is given by

$$U=\int_{\mathcal{R}}Wdv, \quad (7)$$

where $\mathcal{R}=[0,L_1]\times[0,L_2]\times[0,L_3]$. The displacement or traction components and electric potential or normal component of the electric displacement on the edges $x_1=0, L_1$; $x_2=0, L_2$; and on the bottom and top surfaces are specified as

$$\mathbf{I}_{u\phi}^{(s)}\begin{bmatrix} \mathbf{u} \\ \phi \end{bmatrix}+\mathbf{I}_{\sigma D}^{(s)}\begin{bmatrix} \boldsymbol{\sigma}_s \\ D_s \end{bmatrix}=\mathbf{f}^{(s)} \quad \text{on } x_s=0, \quad (s=1,2,3), \quad (8)$$

$$\mathbf{J}_{u\phi}^{(s)}\begin{bmatrix} \mathbf{u} \\ \phi \end{bmatrix}+\mathbf{J}_{\sigma D}^{(s)}\begin{bmatrix} \boldsymbol{\sigma}_s \\ D_s \end{bmatrix}=\mathbf{g}^{(s)} \quad \text{on } x_s=L_s,$$

where $(\boldsymbol{\sigma}_s)_i=\sigma_{is}$. The functions $\mathbf{f}^{(s)}, \mathbf{g}^{(s)}$ are known and $\mathbf{I}_{u\phi}^{(s)}, \mathbf{I}_{\sigma D}^{(s)}, \mathbf{J}_{u\phi}^{(s)}, \mathbf{J}_{\sigma D}^{(s)}$ are 4×4 diagonal matrices. For most applications, these diagonal matrices have entries either zero or one such that

$$\mathbf{I}_{u\phi}^{(s)}+\mathbf{I}_{\sigma D}^{(s)}=\mathbf{J}_{u\phi}^{(s)}+\mathbf{J}_{\sigma D}^{(s)}=\mathbf{I} \quad (s=1,2,3), \quad (9)$$

with \mathbf{I} being the 4×4 identity matrix. For example, if the surface $x_1=0$ is rigidly clamped and electrically grounded then $\mathbf{I}_{u\phi}^{(1)}=\mathbf{I}$, $\mathbf{I}_{\sigma D}^{(1)}=\mathbf{0}$ and $\mathbf{f}^{(1)}(x_2, x_3)=\mathbf{0}$, i.e., $u_1=u_2=u_3=0, \phi=0$. If the surface is rigidly clamped and the normal component of the electric displacement is zero, then $\mathbf{I}_{u\phi}^{(1)}=\text{diag}[1,1,1,0]$, $\mathbf{I}_{\sigma D}^{(1)}=\text{diag}[0,0,0,1]$. Boundary conditions at an electrically grounded simply supported edge $x_1=0$ may be simulated by $\mathbf{I}_{u\phi}^{(1)}=\text{diag}[0,1,1,1]$, $\mathbf{I}_{\sigma D}^{(1)}=\text{diag}[1,0,0,0]$ and $\mathbf{f}^{(1)}(x_2, x_3)=\mathbf{0}$, i.e., $u_2=u_3=0, \phi=0$ and $\sigma_{11}=0$. The method is valid even when the elements of matrices $\mathbf{I}_{u\phi}^{(s)}, \mathbf{I}_{\sigma D}^{(s)}, \mathbf{J}_{u\phi}^{(s)}$ and $\mathbf{J}_{\sigma D}^{(s)}$ are functions of coordinates only.

The interface conditions on the material surfaces $x_3=L_3^{(2)}, \dots, L_3^{(n)}, \dots, L_3^{(N)}$ may be specified as follows:

(a) If the surface $x_3=L_3^{(n)}$ is an interface between two laminae, the mechanical displacements, surface tractions, electric potential, and the normal component of the electric displacement between them are taken to be continuous. That is

$$\llbracket \mathbf{u} \rrbracket = \mathbf{0}, \llbracket \boldsymbol{\sigma}_3 \rrbracket = \mathbf{0}, \llbracket \phi \rrbracket = 0, \llbracket D_3 \rrbracket = 0 \quad \text{on } x_3=L_3^{(n)}. \quad (10)$$

Here $\llbracket \mathbf{u} \rrbracket$ denotes the jump in the value of \mathbf{u} across an interface. Thus the adjoining laminae are presumed to be perfectly bonded together.

(b) If the surface $x_3=L_3^{(n)}$ is an electroded interface, then the potential on this surface is a known function $f(x_1, x_2)$ while the normal component of the electric displacement need not be continuous across this interface, i.e.,

$$\llbracket \mathbf{u} \rrbracket = \mathbf{0}, \llbracket \boldsymbol{\sigma}_3 \rrbracket = \mathbf{0}, \phi=f(x_1, x_2) \quad \text{on } x_3=L_3^{(n)}. \quad (11)$$

We assume that the electrode is of infinitesimal thickness and ignore its influence on the mechanical deformations of the structure.

3 A Solution of the Governing Differential Equations

We construct a local coordinate system $x_1^{(n)}, x_2^{(n)}, x_3^{(n)}$ with local axes parallel to the global axes and the origin at the point where the global x_3 -axis intersects the bottom surface of the n th lamina. In this local coordinate system, the n th lamina occupies the region $[0, l_1]\times[0, l_2]\times[0, l_3^{(n)}]$, where $l_1=L_1, l_2=L_2$ and $l_3^{(n)}=L_3^{(n+1)}-L_3^{(n)}$. We drop the superscript n for convenience with the understanding that all material constants and variables belong to this lamina.

The Eshelby-Stroh formalism ([24–26]) provides a solution for the generalized plane-strain deformations of a linear elastic/piezoelectric anisotropic material. We extend it to three-dimensional deformations by assuming that

$$\begin{bmatrix} \mathbf{u} \\ \phi \end{bmatrix}=\mathbf{a}\exp\left[i\left(\frac{k_1\pi}{l_1}x_1+\frac{k_2\pi}{l_2}x_2+p\frac{x_3}{l_3}\right)\right], \quad (12)$$

where \mathbf{a} and p are possible complex constants to be determined, k_1 and k_2 are known integers, and $i=\sqrt{-1}$. The chosen displacement and potential field has a sinusoidal variation on the x_1-x_2

plane with an arbitrary exponential variation in the x_3 -direction; k_1 and k_2 determine the period of the sinusoidal terms in the x_1 and x_2 -directions respectively.

From Eqs. (12), (3), and (2) we obtain

$$\begin{aligned} \sigma_{jm} &= i(C_{jmqra_q} + e_{rjm}a_4) \left(\frac{k_1\pi}{l_1} \delta_{r1} + \frac{k_2\pi}{l_2} \delta_{r2} + p \frac{\delta_{r3}}{l_3} \right) \\ &\quad \times \exp \left[i \left(\frac{k_1\pi}{l_1} x_1 + \frac{k_2\pi}{l_2} x_2 + p \frac{x_3}{l_3} \right) \right], \\ D_m &= i(e_{mqr}a_q - \epsilon_{mr}a_4) \left(\frac{k_1\pi}{l_1} \delta_{r1} + \frac{k_2\pi}{l_2} \delta_{r2} + p \frac{\delta_{r3}}{l_3} \right) \\ &\quad \times \exp \left[i \left(\frac{k_1\pi}{l_1} x_1 + \frac{k_2\pi}{l_2} x_2 + p \frac{x_3}{l_3} \right) \right]. \end{aligned} \quad (13)$$

Here δ_{ij} is the Kronecker delta ([30]). Substitution of (13) into (1) gives equations which can be written as

$$\begin{aligned} \{\mathbf{Q}^C + p[\mathbf{R}^C + (\mathbf{R}^C)^T] + p^2\mathbf{T}^C\} \mathbf{a}^C + \{\mathbf{q}^e + p[\mathbf{r}^e + \mathbf{s}^e] + p^2\mathbf{t}^e\} a_4 &= \mathbf{0}, \\ \{(\mathbf{q}^e)^T + p[(\mathbf{r}^e)^T + (\mathbf{s}^e)^T] + p^2(\mathbf{t}^e)^T\} \mathbf{a}^C - \{q^\epsilon + p[r^\epsilon + s^\epsilon] + p^2t^\epsilon\} a_4 &= 0, \end{aligned} \quad (14)$$

where $\mathbf{a}^C = [a_1, a_2, a_3]^T$, the matrices $\mathbf{Q}^C, \mathbf{R}^C, \mathbf{T}^C$ are related to the elastic constants C_{jmqr} by

$$\begin{aligned} Q_{jq}^C &= \frac{k_1^2\pi^2}{l_1^2} C_{j1q1} + \frac{k_1k_2\pi^2}{l_1l_2} (C_{j1q2} + C_{j2q1}) + \frac{k_2^2\pi^2}{l_2^2} C_{j2q2}, \\ R_{jq}^C &= \frac{k_1\pi}{l_3l_1} C_{j3q1} + \frac{k_2\pi}{l_3l_2} C_{j3q2}, \quad T_{jq}^C = \frac{1}{l_3^2} C_{j3q3}, \end{aligned} \quad (15)$$

the vectors $\mathbf{q}^e, \mathbf{r}^e, \mathbf{s}^e$, and \mathbf{t}^e are related to the piezoelectric moduli e_{rjm} by

$$\begin{aligned} q_j^e &= \frac{k_1^2\pi^2}{l_1^2} e_{1j1} + \frac{k_1k_2\pi^2}{l_1l_2} (e_{1j2} + e_{2j1}) + \frac{k_2^2\pi^2}{l_2^2} e_{2j2}, \\ r_j^e &= \frac{k_1\pi}{l_3l_1} e_{3j1} + \frac{k_2\pi}{l_3l_2} e_{3j2}, \quad s_j^e = \frac{k_1\pi}{l_3l_1} e_{1j3} + \frac{k_2\pi}{l_3l_2} e_{2j3}, \\ t_j^e &= \frac{1}{l_3^2} e_{3j3}, \end{aligned} \quad (16)$$

and the scalars $q^\epsilon, r^\epsilon, s^\epsilon$, and t^ϵ are related to the electric permittivity ϵ_{jr} by

$$\begin{aligned} q^\epsilon &= \frac{k_1^2\pi^2}{l_1^2} \epsilon_{11} + \frac{k_1k_2\pi^2}{l_1l_2} (\epsilon_{12} + \epsilon_{21}) + \frac{k_2^2\pi^2}{l_2^2} \epsilon_{22}, \\ r^\epsilon &= \frac{k_1\pi}{l_3l_1} \epsilon_{31} + \frac{k_2\pi}{l_3l_2} \epsilon_{32}, \quad s^\epsilon = \frac{k_1\pi}{l_3l_1} \epsilon_{13} + \frac{k_2\pi}{l_3l_2} \epsilon_{23}, \quad t^\epsilon = \frac{1}{l_3^2} \epsilon_{33}. \end{aligned} \quad (17)$$

It should be noted that $s^\epsilon = r^\epsilon$ due to the symmetry restriction (5)₃ on the electric permittivity tensor. The two equations in (14) can be combined as

$$\{\mathbf{Q} + p[\mathbf{R} + \mathbf{R}^T] + p^2\mathbf{T}\} \mathbf{a} = \mathbf{0}, \quad (18)$$

where

$$\mathbf{Q} = \begin{bmatrix} \mathbf{Q}^C & \mathbf{q}^e \\ (\mathbf{q}^e)^T & -q^\epsilon \end{bmatrix}, \quad \mathbf{R} = \begin{bmatrix} \mathbf{R}^C & \mathbf{r}^e \\ (\mathbf{r}^e)^T & -r^\epsilon \end{bmatrix}, \quad \mathbf{T} = \begin{bmatrix} \mathbf{T}^C & \mathbf{t}^e \\ (\mathbf{t}^e)^T & -t^\epsilon \end{bmatrix}. \quad (19)$$

Following the method used by Suo et al. [31] for generalized plane deformations of piezoelectric materials, we can prove that the eigenvalues p of (18) cannot be real. Since the matrices \mathbf{Q}, \mathbf{R} , and \mathbf{T} in (18) are real, there are four pairs of complex conjugate values for p . Let $(p_\alpha, \mathbf{a}_\alpha)$ ($\alpha = 1, 2, \dots, 8$) be eigensolutions of (18) such that

$$\text{Im}(p_\alpha) > 0, \quad p_{\alpha+4} = \bar{p}_\alpha, \quad \mathbf{a}_{\alpha+4} = \bar{\mathbf{a}}_\alpha \quad (\alpha = 1, \dots, 4), \quad (20)$$

where a bar superimposed on a quantity denotes its complex conjugate. For distinct p_α we can superpose eight solutions of the form (12) to obtain

$$\begin{bmatrix} \mathbf{u} \\ \phi \end{bmatrix} = \mathbf{A} \left\langle \exp \left[i \left(\frac{k_1\pi}{l_1} x_1 + \frac{k_2\pi}{l_2} x_2 + p_* \frac{x_3}{l_3} \right) \right] \right\rangle \mathbf{c} + \text{conjugate}, \quad (21)$$

where $\mathbf{A} = [\mathbf{a}_1, \mathbf{a}_2, \mathbf{a}_3, \mathbf{a}_4]$, \mathbf{c} is an arbitrary 4×1 vector of unknown complex coefficients, $\langle \psi(p_*) \rangle = \text{diag}[\psi(p_1), \psi(p_2), \psi(p_3), \psi(p_4)]$, and conjugate stands for the complex conjugate of the explicitly stated term. We obtain the following expressions for the stress tensor and electric displacement by superposing eight solutions of the form (13),

$$\begin{bmatrix} \boldsymbol{\sigma}_m \\ D_m \end{bmatrix} = \mathbf{S}_m \left\langle \exp \left[i \left(\frac{k_1\pi}{l_1} x_1 + \frac{k_2\pi}{l_2} x_2 + p_* \frac{x_3}{l_3} \right) \right] \right\rangle \mathbf{c} + \text{conjugate}, \quad (22)$$

where

$$\begin{aligned} \mathbf{S}_m &= [\mathbf{V}_{(m,1)} \mathbf{a}_1, \mathbf{V}_{(m,2)} \mathbf{a}_2, \mathbf{V}_{(m,3)} \mathbf{a}_3, \mathbf{V}_{(m,4)} \mathbf{a}_4], \\ \mathbf{V}_{(m,\alpha)} &= \begin{bmatrix} \mathbf{V}_{(m,\alpha)}^C & \mathbf{v}_{(m,\alpha)}^e \\ (\mathbf{w}_{(m,\alpha)}^e)^T & -v_{(m,\alpha)}^\epsilon \end{bmatrix}, \\ (\mathbf{V}_{(m,\alpha)}^C)_{jq} &= i \left(\frac{k_1\pi}{l_1} C_{jm q1} + \frac{k_2\pi}{l_2} C_{jm q2} + p_\alpha \frac{C_{jm q3}}{l_3} \right), \\ (\mathbf{v}_{(m,\alpha)}^e)_j &= i \left(\frac{k_1\pi}{l_1} e_{1jm} + \frac{k_2\pi}{l_2} e_{2jm} + p_\alpha \frac{e_{3jm}}{l_3} \right), \\ (\mathbf{w}_{(m,\alpha)}^e)_j &= i \left(\frac{k_1\pi}{l_1} e_{mj1} + \frac{k_2\pi}{l_2} e_{mj2} + p_\alpha \frac{e_{mj3}}{l_3} \right), \\ v_{(m,\alpha)}^\epsilon &= i \left(\frac{k_1\pi}{l_1} \epsilon_{m1} + \frac{k_2\pi}{l_2} \epsilon_{m2} + p_\alpha \frac{\epsilon_{m3}}{l_3} \right). \end{aligned} \quad (23)$$

The expressions (21) and (22) are valid when the eigenvalues p_α are distinct, or if they are not, there exist eight independent eigenvectors \mathbf{a}_α . If an eigenvalue is repeated r times ($2 \leq r \leq 4$) and it does not have r corresponding independent eigenvectors, then (21) and (22) need to be modified appropriately. The procedure is similar to that given for elastic laminates by Vel and Batra [29].

4 A Series Solution

The complete double Fourier series expansion constructed to satisfy the boundary/interface conditions on the surfaces $x_3^{(n)} = 0, l_3^{(n)}$ is obtained by superposing solutions of the form (21). In the following equations the first superscript n denotes the n th lamina and the second superscript 3 indicates that the series terms have a double Fourier series expansion on the planes $x_3^{(n)} = 0$ and $l_3^{(n)}$. The dependence of the eigenvalues and eigenvectors on k_1 and k_2 is indicated by the subscripts.

$$\begin{aligned} \begin{bmatrix} \mathbf{u}^{(n,3)} \\ \phi^{(n,3)} \end{bmatrix} &= \mathbf{A}_{(k_0, k_0)}^{(n,3)} [\boldsymbol{\eta}_{(k_0, k_0)}^{(n,3)} \mathbf{c}_{(k_0, k_0)}^{(n,3)} + \boldsymbol{\xi}_{(k_0, k_0)}^{(n,3)} \mathbf{d}_{(k_0, k_0)}^{(n,3)}] + \sum_{k_1=1}^{\infty} \mathbf{A}_{(k_1, 0)}^{(n,3)} \\ &\quad \times [\boldsymbol{\eta}_{(k_1, 0)}^{(n,3)} \mathbf{c}_{(k_1, 0)}^{(n,3)} + \boldsymbol{\xi}_{(k_1, 0)}^{(n,3)} \mathbf{d}_{(k_1, 0)}^{(n,3)}] + \sum_{k_2=1}^{\infty} \mathbf{A}_{(0, k_2)}^{(n,3)} [\boldsymbol{\eta}_{(0, k_2)}^{(n,3)} \mathbf{c}_{(0, k_2)}^{(n,3)} \\ &\quad + \boldsymbol{\xi}_{(0, k_2)}^{(n,3)} \mathbf{d}_{(0, k_2)}^{(n,3)}] + \sum_{k_1, k_2=1}^{\infty} \{\mathbf{A}_{(k_1, k_2)}^{(n,3)} [\boldsymbol{\eta}_{(k_1, k_2)}^{(n,3)} \mathbf{c}_{(k_1, k_2)}^{(n,3)} \\ &\quad + \boldsymbol{\xi}_{(k_1, k_2)}^{(n,3)} \mathbf{d}_{(k_1, k_2)}^{(n,3)}] + \mathbf{A}_{(k_1, -k_2)}^{(n,3)} [\boldsymbol{\eta}_{(k_1, -k_2)}^{(n,3)} \mathbf{c}_{(k_1, -k_2)}^{(n,3)} \\ &\quad + \boldsymbol{\xi}_{(k_1, -k_2)}^{(n,3)} \mathbf{d}_{(k_1, -k_2)}^{(n,3)}]\} + \text{conjugate}. \end{aligned} \quad (24)$$

The terms involving $k_0 \in (0,1)$ play the role of the constant term in the double Fourier series expansion and

$$\begin{aligned} \boldsymbol{\eta}_{(k_1, k_2)}^{(n,3)}(x_1^{(n)}, x_2^{(n)}, x_3^{(n)}) &= \left\langle \exp \left[i \left(\frac{k_1 \pi}{l_1} x_1^{(n)} + \frac{k_2 \pi}{l_2} x_2^{(n)} \right. \right. \right. \\ &\quad \left. \left. \left. + P_{(k_1, k_2, *)}^{(n,3)} \frac{x_3^{(n)}}{l_3^{(n)}} \right) \right] \right\rangle, \\ \boldsymbol{\xi}_{(k_1, k_2)}^{(n,3)}(x_1^{(n)}, x_2^{(n)}, x_3^{(n)}) &= \left\langle \exp \left[-i \left(\frac{k_1 \pi}{l_1} x_1^{(n)} + \frac{k_2 \pi}{l_2} x_2^{(n)} \right. \right. \right. \\ &\quad \left. \left. \left. + P_{(k_1, k_2, *)}^{(n,3)} \left(\frac{x_3^{(n)}}{l_3^{(n)}} - 1 \right) \right) \right] \right\rangle. \end{aligned} \quad (25)$$

The functions $\boldsymbol{\eta}_{(k_1, k_2)}^{(n,3)}(x_1^{(n)}, x_2^{(n)}, x_3^{(n)})$ and $\boldsymbol{\xi}_{(k_1, k_2)}^{(n,3)}(x_1^{(n)}, x_2^{(n)}, x_3^{(n)})$ vary sinusoidally on the surfaces $x_3^{(n)}=0, l_3^{(n)}$ and exponentially in the $x_3^{(n)}$ -direction. The inequality (20)₁ ensures that all functions decay exponentially towards the interior of the n th lamina.

Similar expressions can be written for $[\mathbf{u}^{(n,1)}, \boldsymbol{\phi}^{(n,1)}]^T$ and $[\mathbf{u}^{(n,2)}, \boldsymbol{\phi}^{(n,2)}]^T$ which have a complete double Fourier series expansion on the side surfaces $x_1^{(n)}=0, l_1$ and $x_2^{(n)}=0, l_2$ respectively. The mechanical displacement, electric potential, stress, and electric displacement fields for the n th lamina are

$$\begin{bmatrix} \mathbf{u}^{(n)} \\ \boldsymbol{\phi}^{(n)} \end{bmatrix} = \sum_{s=1}^3 \begin{bmatrix} \mathbf{u}^{(n,s)} \\ \boldsymbol{\phi}^{(n,s)} \end{bmatrix}, \quad \begin{bmatrix} \boldsymbol{\sigma}_m^{(n)} \\ \mathbf{D}_m^{(n)} \end{bmatrix} = \sum_{s=1}^3 \begin{bmatrix} \boldsymbol{\sigma}_m^{(n,s)} \\ \mathbf{D}_m^{(n,s)} \end{bmatrix}. \quad (26)$$

The unknowns $\mathbf{c}_{(k_1, k_2)}^{(n,s)}$ and $\mathbf{d}_{(k_1, k_2)}^{(n,s)}$ in (26) are assumed to be complex, except for $\mathbf{c}_{(k_0, k_0)}^{(n,s)}$ and $\mathbf{d}_{(k_0, k_0)}^{(n,s)}$ which are real.

5 Satisfaction of Boundary and Interface Conditions

The boundary conditions (8) on the surfaces $x_s=0, L_s$ and continuity conditions (10) or (11) on the interfaces $x_3=L_3^{(2)}, L_3^{(3)}, \dots, L_3^{(N)}$ are satisfied by the classical Fourier series method, resulting in a system of linear algebraic equations for the unknown coefficients $\mathbf{c}_{(k_1, k_2)}^{(n,s)}$ and $\mathbf{d}_{(k_1, k_2)}^{(n,s)}$. On the bottom surface $x_3^{(1)}=0$, we extend the component functions in (26) defined on $[0, l_1] \times [0, l_2]$ to the interval $[-l_1, l_1] \times [-l_2, l_2]$. The functions $\boldsymbol{\eta}_{(k_1, k_2)}^{(1,3)}$ and $\boldsymbol{\xi}_{(k_1, k_2)}^{(1,3)}$ which have a sinusoidal variation on the plane $x_3^{(1)}=0$ are extended without modification since they form the basis functions for this surface, except for terms involving k_0 which are extended as even functions. The functions $\boldsymbol{\eta}_{(k_1, k_2)}^{(1,1)}$ and $\boldsymbol{\xi}_{(k_1, k_2)}^{(1,1)}$ which have an exponential variation in the $x_1^{(1)}$ -direction and a sinusoidal variation in the $x_2^{(1)}$ -direction are extended as even functions in the $x_1^{(1)}$ -direction and without modification in the $x_2^{(1)}$ -direction. The functions $\boldsymbol{\eta}_{(k_1, k_2)}^{(1,2)}$ and $\boldsymbol{\xi}_{(k_1, k_2)}^{(1,2)}$ are extended as even functions in the $x_2^{(1)}$ -direction and without modification in the $x_1^{(1)}$ -direction. The prescribed function $\mathbf{f}^{(3)}(x_1^{(1)}, x_2^{(1)})$ is suitably extended. We multiply (8)₁ corresponding to $s=3$ by $\exp[i(\bar{k}_1 \pi x_1^{(1)}/l_1 + \bar{k}_2 \pi x_2^{(1)}/l_2)]$ and integrate the result with respect to $x_1^{(1)}$ and $x_2^{(1)}$ over the interval $[-l_1, l_1] \times [-l_2, l_2]$ to obtain

$$\begin{aligned} \int_{-l_2}^{l_2} \int_{-l_1}^{l_1} \left\{ \mathbf{I}_{u\phi}^{(3)} \begin{bmatrix} \mathbf{u}^{(1)} \\ \boldsymbol{\phi}^{(1)} \end{bmatrix} + \mathbf{I}_{\sigma D}^{(3)} \begin{bmatrix} \boldsymbol{\sigma}_3^{(1)} \\ \mathbf{D}_3^{(1)} \end{bmatrix} - \mathbf{f}^{(3)} \right\} \\ \times \exp \left[i \left(\frac{\bar{k}_1 \pi x_1^{(1)}}{l_1} + \frac{\bar{k}_2 \pi x_2^{(1)}}{l_2} \right) \right] dx_1^{(1)} dx_2^{(1)} = \mathbf{0} \quad \text{at } x_3^{(1)}=0, \end{aligned} \quad (27)$$

for all $(\bar{k}_1, \bar{k}_2) \in (\{0\}, \{0\}) \cup (\mathcal{Z}^+ \times \{0\}) \cup (\{0\} \times \mathcal{Z}^+) \cup (\mathcal{Z}^+ \times \mathcal{Z}^+) \cup (\mathcal{Z}^+ \times \mathcal{Z}^-)$, where \mathcal{Z}^+ and \mathcal{Z}^- denote the sets of positive and negative integers, respectively. The same procedure is re-

peated for the boundary condition (8)₂ on the top surface of the N th lamina with $s=3$ and the interface continuity conditions (10) or (11) between the various laminae.

On the side surfaces $x_1^{(n)}=0, l_1$ the functions are extended over the interval $[-l_2, l_2] \times [-l_3^{(n)}, l_3^{(n)}]$ in the $x_2^{(n)}-x_3^{(n)}$ plane. We then multiply (8) corresponding to $s=1$ by $\exp[i(\bar{k}_2 \pi x_2^{(n)}/l_2 + \bar{k}_3 \pi x_3^{(n)}/l_3^{(n)})]$ and integrate the result with respect to $x_2^{(n)}$ and $x_3^{(n)}$ over $[-l_2, l_2] \times [-l_3^{(n)}, l_3^{(n)}]$. A similar procedure is used to satisfy the boundary conditions (8) corresponding to $s=2$ on the surfaces $x_2^{(n)}=0, l_2$.

Substitution from (26) into (27) and the other equations that enforce the boundary conditions on the top surface, the interfaces between adjoining laminae and the side surfaces leads to an infinite set of linear algebraic equations for the infinitely many unknown coefficients $\mathbf{c}_{(k_1, k_2)}^{(n,s)}$ and $\mathbf{d}_{(k_1, k_2)}^{(n,s)}$. A general theory for the solution of the resulting infinite system of equations does not exist. However, reasonably accurate results can be obtained by truncating k_1 and k_2 in (24) to K_1 and K_2 terms, respectively. The series involving summations over k_1 and k_2 in the expression for $[\mathbf{u}^{(n,1)}, \boldsymbol{\phi}^{(n,1)}]$ are truncated to K_2 and $K_3^{(n)}$ while those for $[\mathbf{u}^{(n,2)}, \boldsymbol{\phi}^{(n,2)}]$ are truncated to $K_3^{(n)}$ and K_1 terms. In general, we try to maintain approximately the same period of the largest harmonic on all interfaces and boundaries by choosing $K_3^{(n)} = \text{Ceil}(K_1 l_3^{(n)}/l_1)$ and $K_2 = \text{Ceil}(K_1 l_2/l_1)$, where $\text{Ceil}(y)$ equals the smallest integer greater than or equal to y . Thus, the size of the truncated matrix will depend solely on the choice of K_1 .

6 Results and Discussion

Problems studied by Heyliger [20] and Heyliger et al. [10] were analyzed by the present method with $K_1=200$, and the two sets of results matched very well. As shown below, satisfactory results can be computed even with $K_1=50$.

We present results for laminated plates with each lamina made of either graphite-epoxy ([22]), PVDF ([10,32]) or PZT-5A ([22]) with nonzero values of material variables listed in Table 1. We treat the graphite-epoxy layer as a piezoelectric material with the piezoelectric moduli set equal to zero, and solve for the electric field in the graphite-epoxy layer which is uncoupled from the elastic field. In this section we denote the thickness of the lamina by $H(=L_3)$.

Although our solution is applicable to laminates with general boundary conditions on all four edges, here we consider laminated piezoelectric plates that are simply supported and electrically grounded on the opposite edges $x_2=0$ and L_2 , i.e., $u_1=u_3=0$, $\sigma_{22}=0$, $\phi=0$, and the other two edges subjected to various boundary conditions. The reason for this choice is that if each

Table 1 Nonvanishing material properties of the graphite-epoxy, PVDF, and PZT-5A

Property	0° Graphite-epoxy	0° PVDF	PZT-5A
C_{1111} (GPa)	183.443	238.24	99.201
C_{2222} (GPa)	11.662	23.60	99.201
C_{3333} (GPa)	11.662	10.64	86.856
C_{1122} (GPa)	4.363	3.98	54.016
C_{1133} (GPa)	4.363	2.19	50.778
C_{2233} (GPa)	3.918	1.92	50.778
C_{2323} (GPa)	2.870	2.15	21.100
C_{3131} (GPa)	7.170	4.40	21.100
C_{1212} (GPa)	7.170	6.43	22.593
e_{311} (Cm ⁻²)	0	-0.130	-7.209
e_{322} (Cm ⁻²)	0	-0.145	-7.209
e_{333} (Cm ⁻²)	0	-0.276	15.118
e_{223} (Cm ⁻²)	0	-0.009	12.322
e_{113} (Cm ⁻²)	0	-0.135	12.322
ϵ_{11} (10 ⁻¹⁰ F/m)	153.0	1.1068	153.0
ϵ_{22} (10 ⁻¹⁰ F/m)	153.0	1.0607	153.0
ϵ_{33} (10 ⁻¹⁰ F/m)	153.0	1.0607	150.0

Table 2 Convergence study for a [0 deg PVDF/90 deg PVDF] square laminate subjected to mechanical load, $L_1/H=5$

K_1	$\tilde{u}_1(H)$	$\tilde{u}_3(H^\pm/2)$	$\tilde{\sigma}_{11}(H)$	$\tilde{\sigma}_{13}(H^\pm/2)$	$\tilde{\phi}(3H/4)$	$\tilde{D}_3(H)$	\tilde{U}
25	-0.244 744	6.803 677	1.690 039	0.232 611	-0.221 222	2.784 989	1.028 037
		6.803 467		0.232 731			
50	-0.244 314	6.803 253	1.676 032	0.233 188	-0.220 854	2.758 772	1.028 027
		6.803 291		0.233 036			
100	-0.244 253	6.803 264	1.681 768	0.232 722	-0.220 854	2.772 986	1.028 026
		6.803 255		0.232 736			
150	-0.244 243	6.803 245	1.678 181	0.232 879	-0.220 851	2.764 628	1.028 026
		6.803 250		0.232 921			
200	-0.244 237	6.803 248	1.680 697	0.233 243	-0.220 850	2.770 503	1.028 025
		6.803 245		0.233 243			

lamina is made of a monoclinic material of crystal class m (see [33]), then the boundary conditions at the edges $x_2=0, L_2$ are identically satisfied by the following mechanical displacement and electric potential distributions:

$$\mathbf{u} = [f_1(x_1, x_3) \sin(\lambda \pi x_2 / L_2), f_2(x_1, x_3) \times \cos(\lambda \pi x_2 / L_2), f_3(x_1, x_3) \sin(\lambda \pi x_2 / L_2)]^T$$

$$\phi = f_4(x_1, x_3) \sin(\lambda \pi x_2 / L_2). \quad (28)$$

The equilibrium and charge equations will yield coupled partial differential equations for $f_\alpha(x_1, x_3)$, ($\alpha=1, \dots, 4$). Thus, we need only one term, namely $k_2=\lambda$, in the x_2 -direction in the double Fourier series expansion and the size of the truncated matrix is greatly reduced. PVDF and graphite-epoxy are orthorhombic materials of crystal class mm2 and PZT-5A is a hexagonal material of crystal class 6mm, all of which belong to the group of monoclinic materials of crystal class m.

The edges $x_1=0, L_1$ may be either clamped (C) with $u_1=u_2=u_3=0$, or free of traction (F) with $\sigma_{11}=\sigma_{12}=\sigma_{13}=0$ or simply supported (S) with $u_1=u_3=0, \sigma_{11}=0$. We append P when the edge is electrically grounded ($\phi=0$) or D when the normal component of the electric displacement is set to zero, i.e., $D_1=0$. For example, FP-FP denotes a laminated plate that is traction-free and electrically grounded on the edges $x_1=0$ and L_1 . In this notation, all analytical three-dimensional solutions available to date ([18–21]) are for piezoelectric laminates that have all four edges subjected to SP boundary conditions.

6.1 PVDF Cross-Ply Laminate. Consider a two-ply square laminate with the bottom and top layers made of 0 deg PVDF and 90 deg PVDF, respectively. The material properties of the 90 deg PVDF may be inferred from those of the 0 deg PVDF given in Table 1. Both layers are of equal thickness, $L_1/H=5$ and $L_1=1.0$ m. The interface is electroded and conditions (11) are enforced with $f(x_1, x_2)=0$ on $x_3=H/2$. The following two electro-mechanical loading cases are considered:

(i) Mechanical load:

$$\sigma_3(x_1, x_2, H) = [0, 0, q_0/2]^T \sin(\pi x_1 / L_1) \sin(\pi x_2 / L_2) \quad (29)$$

$$\sigma_3(x_1, x_2, 0) = [0, 0, -q_0/2]^T \sin(\pi x_1 / L_1) \sin(\pi x_2 / L_2)$$

$$\phi(x_1, x_2, H) = \phi(x_1, x_2, 0) = 0;$$

(ii) Electrical load:

$$\phi(x_1, x_2, H) = \phi(x_1, x_2, 0) = 0.5 \phi_0 \sin(\pi x_1 / L_1) \sin(\pi x_2 / L_2),$$

$$\sigma_3(x_1, x_2, H) = \sigma_3(x_1, x_2, 0) = 0. \quad (30)$$

Results for combined mechanical and electrical loads can be obtained by superposition of the solutions corresponding to loads (i) and (ii).

The effect of truncation of the series on the accuracy of the solution is investigated for the two-ply laminated plate with two opposite edges simply supported and grounded and the other two edges subjected to FD-FD boundary conditions. Computed results for various quantities at specific points in the laminate are listed in Table 2 for the case of the mechanical loading. The following nondimensionalization has been used:

$$[\tilde{u}_1(x_3), \tilde{u}_3(x_3)] = \frac{C_0}{L_1 q_0} \left[u_1 \left(\frac{L_1}{4}, \frac{L_2}{2}, x_3 \right), u_3 \left(\frac{L_1}{2}, \frac{L_2}{2}, x_3 \right) \right],$$

$$[\tilde{\sigma}_{11}(x_3), \tilde{\sigma}_{13}(x_3)] = \frac{1}{q_0} \left[\sigma_{11} \left(\frac{L_1}{2}, \frac{L_2}{2}, x_3 \right), \sigma_{13} \left(\frac{L_1}{8}, \frac{L_2}{2}, x_3 \right) \right],$$

$$[\tilde{\sigma}_{23}(x_3), \tilde{\sigma}_{33}(x_3)] = \frac{1}{q_0} \left[\sigma_{23} \left(\frac{L_1}{8}, 0, x_3 \right), \sigma_{33} \left(\frac{L_1}{2}, \frac{L_2}{2}, x_3 \right) \right],$$

$$\tilde{\phi}(x_3) = \frac{1000 e_0}{L_1 q_0} \phi \left(\frac{L_1}{2}, \frac{L_2}{2}, x_3 \right), \quad (31)$$

$$\tilde{D}_3(x_3) = \frac{C_0}{e_0 q_0} D_3 \left(\frac{L_1}{2}, \frac{L_2}{2}, x_3 \right),$$

$$\tilde{U} = \frac{U C_0}{q_0^2 L_1^3},$$

where $C_0=23.60$ GPa and $e_0=-0.145$ Cm⁻² are representative values of the elastic and piezoelectric moduli for a PVDF (Table

Table 3 Convergence study for a [0 deg PVDF/90 deg PVDF] square laminate subjected to electrical load, $L_1/H=5$

K_1	$\tilde{u}_1(H)$	$\tilde{u}_3(H^\pm/2)$	$\tilde{\sigma}_{11}(0)$	$\tilde{\sigma}_{13}(H^\pm/2)$	$\tilde{\phi}(3H/4)$	$\tilde{D}_3(H)$	\tilde{U}
25	0.664 816	-1.541 948	2.454 258	0.362 439	0.244 276	-6.727 594	0.708 785
		-1.540 149		0.362 538			
50	0.665 182	-1.541 010	2.440 661	0.359 968	0.244 286	-6.791 965	0.708 884
		-1.541 439		0.360 036			
100	0.665 181	-1.541 428	2.454 716	0.362 149	0.244 286	-6.757 952	0.708 908
		-1.541 314		0.361 994			
150	0.665 180	-1.541 397	2.447 524	0.361 835	0.244 286	-6.777 602	0.708 913
		-1.541 450		0.361 693			
200	0.665 201	-1.541 454	2.453 644	0.360 644	0.244 286	-6.763 651	0.708 914
		-1.541 424		0.360 642			

1). These results show that the mechanical displacements \bar{u}_1 and \bar{u}_3 , transverse shear stress $\bar{\sigma}_{13}$ and electric potential $\bar{\phi}$ converge rapidly, but the axial stress $\bar{\sigma}_{11}$ and transverse component \bar{D}_3 of the electric displacement converge slowly. The upper and lower values of the transverse displacement \bar{u}_3 and transverse shear stress $\bar{\sigma}_{13}$ are at corresponding points on the two sides of the interface between the laminae. As is evident, the interface continuity conditions are also satisfied very well with increasing K_1 . The difference in the values of $\bar{\sigma}_{11}(H)$ and $\bar{\sigma}_{11}(H^+/2)$ for $K_1 = 150$ and 200 is 0.15 percent and 0.16 percent, respectively. The total stored energy \bar{U} exhibits monotonic convergence from above and has converged to four decimal places for $K_1 = 50$. While k_0 in (24) was chosen to be 0.5 for this study, a similar convergence behavior was observed for other values of k_0 . Table 3 presents a convergence study for the case of electric loading wherein the nondimensional variables are defined as

$$\begin{aligned} [\hat{u}_1(x_3), \hat{u}_3(x_3)] &= \frac{C_0}{e_0 \phi_0} \left[u_1 \left(\frac{L_1}{4}, \frac{L_2}{2}, x_3 \right), u_3 \left(\frac{L_1}{2}, \frac{L_2}{2}, x_3 \right) \right], \\ [\hat{\sigma}_{11}(x_3), \hat{\sigma}_{13}(x_3)] &= \frac{L_1}{e_0 \phi_0} \left[\sigma_{11} \left(\frac{L_1}{2}, \frac{L_2}{2}, x_3 \right), \sigma_{13} \left(\frac{L_1}{8}, \frac{L_2}{2}, x_3 \right) \right], \\ [\hat{\sigma}_{23}(x_3), \hat{\sigma}_{33}(x_3)] &= \frac{L_1}{e_0 \phi_0} \left[\sigma_{23} \left(\frac{L_1}{8}, 0, x_3 \right), \sigma_{33} \left(\frac{L_1}{8}, \frac{L_2}{2}, x_3 \right) \right], \\ \hat{\phi}(x_3) &= \frac{1}{\phi_0} \phi \left(\frac{L_1}{2}, \frac{L_2}{2}, x_3 \right), \\ \hat{D}_3(x_3) &= \frac{L_1 C_0}{100 e_0^2 \phi_0} D_3 \left(\frac{L_1}{2}, \frac{L_2}{2}, x_3 \right), \quad \hat{U} = \frac{U}{\phi_0^2 \epsilon_0 L_1}. \end{aligned} \quad (32)$$

Here $\epsilon_0 = 1.0607 \times 10^{-10}$ F/m is the typical magnitude of the electric permittivity of a PVDF. In this case too, the mechanical displacements, electric potential, and transverse shear stress converge faster than the longitudinal stress and transverse component of the electric displacement. The total stored energy for the electrical loading converges monotonically from below, in contrast to the case of the mechanical loading where the convergence is from

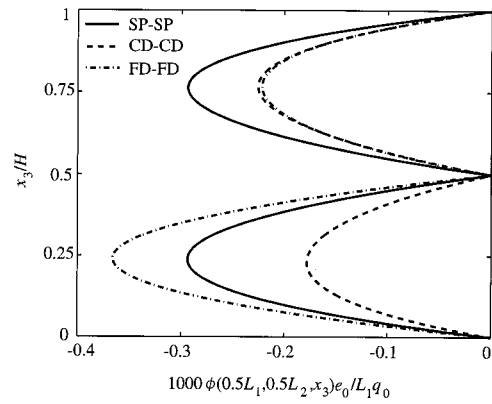


Fig. 2 Influence of the boundary conditions on the through-thickness distribution of the potential due to a mechanical load for the [0 deg PVDF/90 deg PVDF] laminate

above. Thus for the combined mechanical and electrical loading, the total stored energy may not converge monotonically. Results presented below are for $K_1 = 200$.

Electric potential is induced in the laminate due to the application of the mechanical load. The through-thickness distribution of the electric potential at the midspan is shown in Fig. 2 corresponding to three different boundary conditions. The electric potential distribution within each layer is parabolic and the magnitude depends on the boundary condition at the edge. Figure 3 depicts for the mechanical and electric loading the through-thickness distribution of the transverse displacement, longitudinal stress, and transverse shear stress for three different sets of boundary conditions at the edges $x_1 = 0, L_1$. The transverse displacement essentially remains independent of the thickness coordinate for mechanical loading, as is usually assumed in the theory of laminated elastic plates. When subjected to an electric load, the top and bottom surfaces exhibit larger transverse displacement than the midplane. The longitudinal stress σ_{11} is discontinuous across the

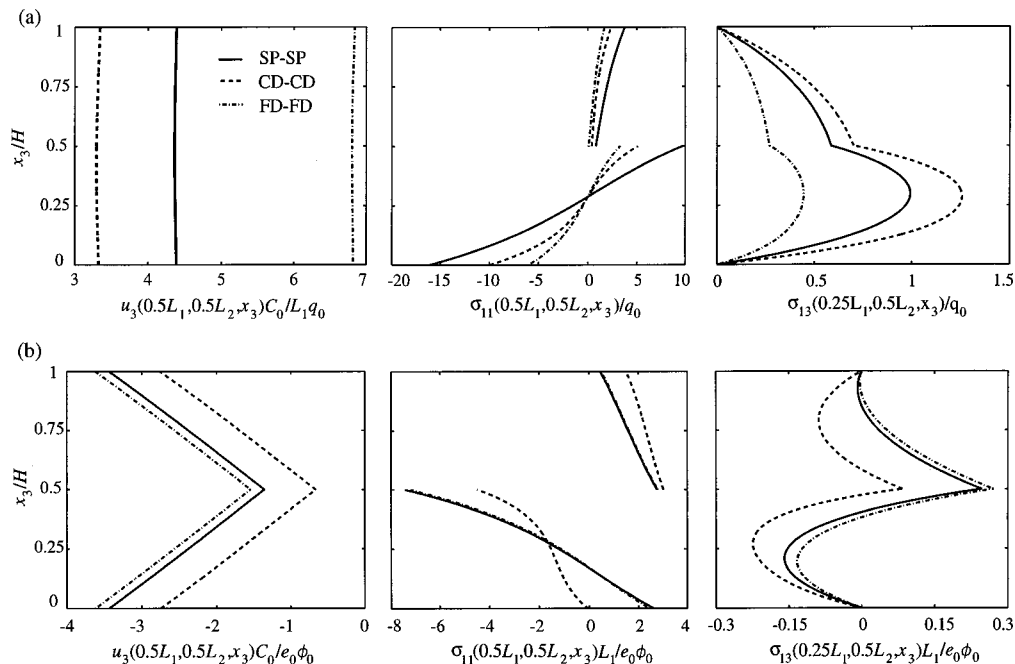


Fig. 3 Influence of the boundary conditions on the through-thickness distribution of the transverse displacement, longitudinal stress, and transverse shear stress for the [0 deg PVDF/90 deg PVDF] laminate subjected to (a) mechanical load and (b) electrical load

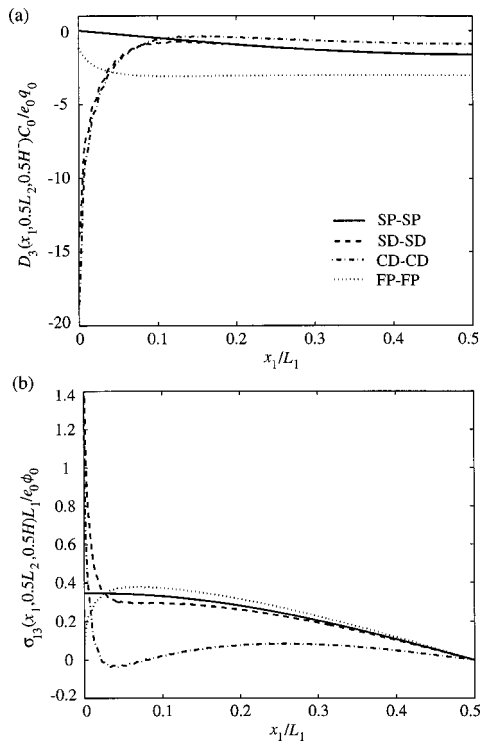


Fig. 4 Axial variation on the interface of the [0 deg PVDF/90 deg PVDF] laminate (a) transverse electric displacement for the mechanical load and (b) transverse shear stress for the electric load

interface due to the change in material properties between the laminae. The longitudinal stress is largest in magnitude on the bottom surface for the mechanical loading and on the 0 deg PVDF side of the interface for the electrical loading. The maximum transverse shear stress σ_{13} occurs at about $x_3 \approx 0.3H$ for the case

of the mechanical loading and is largest when the edges are clamped. When subjected to the electrical load, the maximum transverse shear stress occurs on the interface when the edges are simply supported or traction-free and at $x_3 \approx 0.3H$ when the edges are clamped.

The axial variation of the induced electric displacement component D_3 on the 0 deg PVDF side of the interface is shown in Fig. 4(a) for the mechanical loading. The result is plotted over only half the span since it is symmetric about the midspan. When the edges are simply supported and grounded, i.e., SP boundary conditions, D_3 is largest at the midspan and vanishes at the edges $x_1 = 0, L_1$. In the case of SD and CD boundary conditions, D_3 is essentially uniform over the middle eight-tenth of the span but varies from -19 at $x_1 = 0$ to -1 at $x_1 = 0.1L_1$. This rapid change in D_3 near the edges has not been investigated in detail. The large electric displacements could lead to dielectric failure at the edges when the laminate is subjected to only a moderate mechanical load. The shear stress σ_{13} on the interface due to an electric load is antisymmetric about the midspan and is shown in Fig. 4(b). A thorough study of this rapid change in σ_{13} at the edges except when they are simply supported and grounded, necessitates the use of special functions and has not been pursued here. The shear stress at the edges seems to be singular for SD and CD boundary conditions and could lead to delamination failure at the edges even for moderate electrical loads. Such large stresses were also observed at the edges of piezoelectric layers by Batra et al. [34] and Robbins and Reddy [8].

Figures 5(a) and (b) show the transverse deflection of the midplane for the case of the mechanical and electrical load, respectively, when two of the edges are clamped or traction-free. The transverse deflection of a laminate that is simply supported and electrically grounded on all four edges has the double-sinusoidal shape of the applied mechanical (29) or the electrical load (30), and is not depicted. This is not true when two of the edges are clamped or traction-free. The transverse deflection at the center of the plate is largest when two edges are traction-free and smallest when they are clamped. The transverse deflection near the clamped edges is opposite in direction to that at the center of a

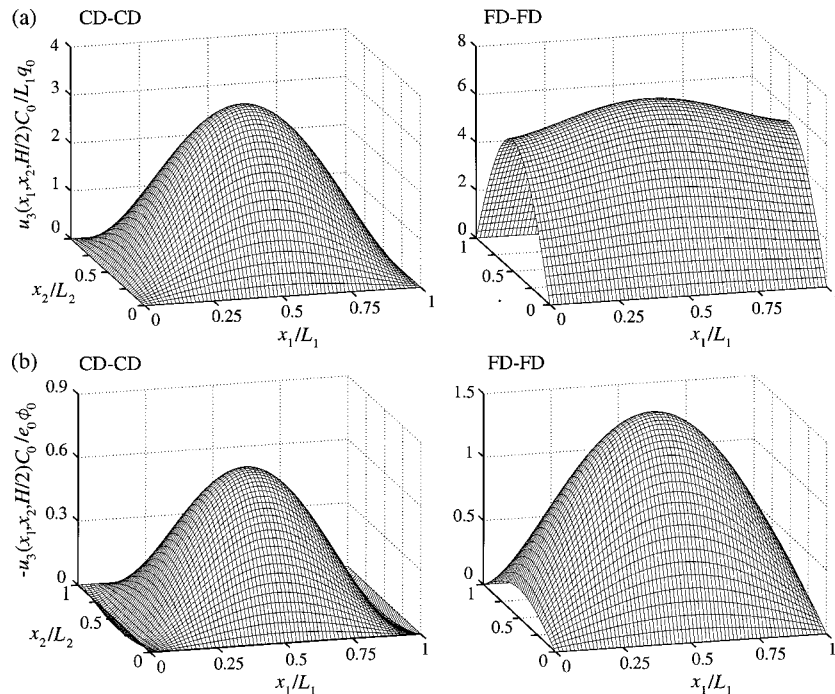


Fig. 5 Influence of the boundary conditions on the midplane transverse displacement of the [0 deg PVDF/90 deg PVDF] laminate for (a) mechanical load and (b) electrical load

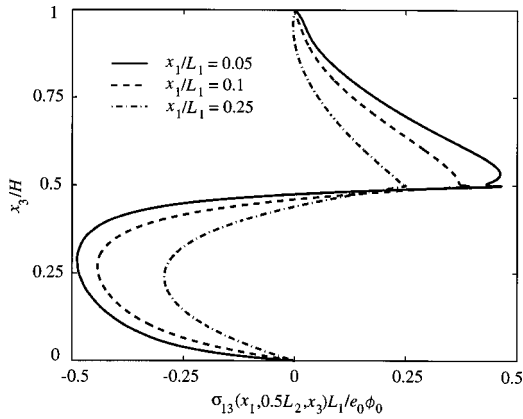


Fig. 6 Through-thickness variation of the transverse shear stress on three sections of a [0 deg PVDF/90 deg PVDF] laminate with layerwise variation of boundary conditions

CD-CD laminate when subjected to the electric load.

The present method can also analyze laminated plates when the edges of each lamina are subjected to boundary conditions different from those on the corresponding edge of the adjoining laminae. As an example, consider the configuration denoted by (CD, FD)-(CD,FD) wherein the bottom lamina of the two-ply laminated plate is clamped at $x_1=0$ and L_1 and the corresponding edges of the top lamina are traction-free with the normal component of the electric displacement set equal to zero for both laminae. Figure 6 depicts the through-thickness distribution of the transverse shear stress σ_{13} on three sections when the laminate is subjected to the electric load. As we approach the edge, the point of the maximum transverse shear stress in the 0 deg PVDF lamina shifts closer to the interface and it is accompanied by large gradients. Numerical results at specific points in the laminate for four sets of boundary conditions given in Table 4 can be used to compare predictions from various plate theories and finite element solutions.

Table 4 Mechanical displacement, stresses, electric potential, and electric displacement at specific locations of a square [0 deg PVDF/90 deg PVDF] laminate for various boundary conditions, $L_1/H=5$

Variable	SP-SP	CD-CD	FD-FD	(CD,FD)-(CD,FD)
$\tilde{u}_1(H)$	-0.785	-0.406	-0.244	-0.617
$\tilde{u}_3(H/2)$	4.360	3.298	6.803	3.676
$\tilde{\sigma}_{11}(H)$	3.770	2.361	1.681	3.080
$\tilde{\sigma}_{13}(H/2)$	0.766	0.902	0.233	0.600
$\tilde{\sigma}_{23}(H/2)$	0.317	0.186	0.908	0.239
$\tilde{\sigma}_{33}(H/2)$	0.000	0.051	-0.089	0.057
$\tilde{\phi}(H/4)$	-0.293	-0.177	-0.365	-0.205
$\tilde{D}_3(0)$	-3.432	-3.147	-4.157	-3.247
$\tilde{u}_1(H)$	0.676	0.382	0.665	0.620
$\tilde{u}_3(H/2)$	-1.357	-0.664	-1.541	-1.046
$\tilde{\sigma}_{11}(0)$	2.642	-0.017	2.454	0.738
$\tilde{\sigma}_{13}(H/2)$	0.321	0.042	0.361	0.376
$\tilde{\sigma}_{23}(H/2)$	0.133	0.232	0.170	0.183
$\tilde{\sigma}_{33}(H/2)$	0.000	0.039	-0.004	-0.094
$\tilde{\phi}(3H/4)$	0.244	0.244	0.244	0.244
$\tilde{D}_3(H)$	-6.770	-6.758	-6.764	-6.762

6.2 Graphite-Epoxy and PZT-5A Hybrid Laminate.

Consider a three-ply square laminate with the bottom and middle layers made of graphite-epoxy with fibers parallel to the x_1 and x_2 directions, respectively, and the topmost layer made of PZT-5A, i.e., [0 deg GE/90 deg GE/PZT-5A]. The graphite-epoxy layers are of thickness $0.4H$, the PZT-5A layer is of thickness $0.2H$, $L_1/H=5$ and $L_1=1.0$ m. Interface conditions (10) are assumed between the graphite-epoxy laminae. The interface between the PZT-5A and its neighboring graphite-epoxy lamina is electroded and grounded. The bottom surface of the laminate is traction-free and the following two electromechanical loadings are considered for the top surface:

- (i) Mechanical load: $\sigma_3(x_1, x_2, H) = [0, 0, q_0]^T \sin(\pi x_1/L_1) \times \sin(\pi x_2/L_2)$, $\phi(x_1, x_2, H) = 0$,
- (ii) Electrical load: $\phi(x_1, x_2, H) = \phi_0 \sin(\pi x_1/L_1) \times \sin(\pi x_2/L_2)$, $\sigma_3(x_1, x_2, H) = \mathbf{0}$.

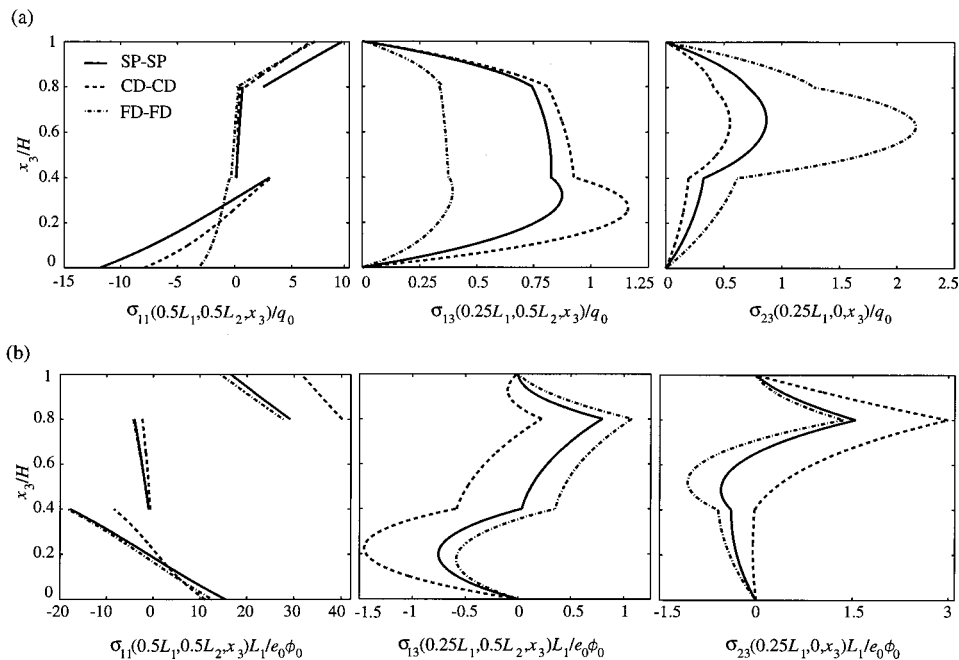


Fig. 7 Influence of the boundary conditions on the through-thickness distribution of the stresses for the [0 deg GE/90 deg GE/PZT-5A] laminate, (a) mechanical load and (b) electrical load

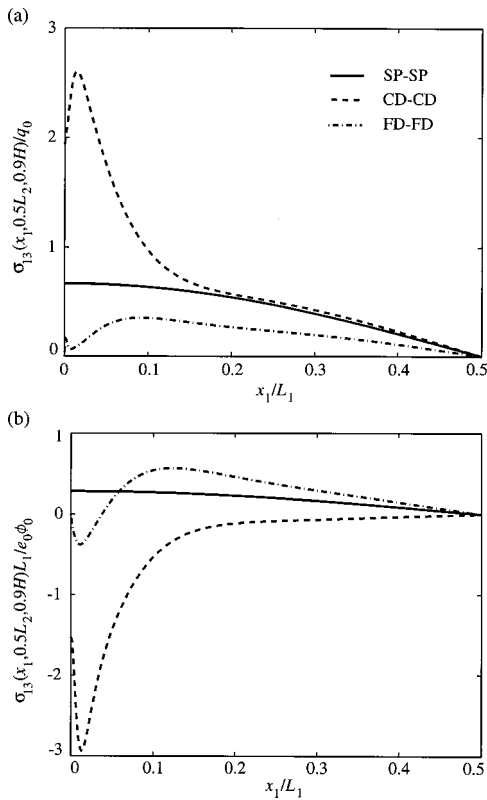


Fig. 8 Axial variation of the transverse shear stress on the midsurface of the PZT-5A lamina of the [0 deg GE/90 deg GE/PZT-5A] laminate for (a) mechanical load and (b) electrical load

The nondimensionalizations (31) and (32) are used with $C_0 = 99.201$ GPa and $e_0 = -7.209$ Cm⁻²; they are representative values of the elastic and piezoelectric moduli of a PZT-5A. Figure 7(a) depicts the through-thickness distribution of stresses for the mechanical loading. The longitudinal stress is approximately piecewise affine. The transverse shear stress σ_{13} is larger when the edges are clamped than when they are simply supported or traction-free. The shear stress σ_{23} attains the maximum value in the 90 deg GE lamina and is largest when the edges are traction-free. The corresponding through-thickness variation of the stresses for the electric loading is shown in Fig. 7(b). The longitudinal stress σ_{11} on the PZT-5A side of the interface is larger than that at other points. The maximum value of the transverse shear stress σ_{13} is at the interface between the PZT and the substrate for simply supported and traction-free boundary conditions and occurs in the 0 deg GE lamina for the clamped boundary condition. The maximum value of the transverse shear stress σ_{23} is at the interface between the PZT and the substrate for all three boundary conditions. Figures 8(a) and (b) show the axial variation of the transverse shear stress σ_{13} on the mid-surface of the PZT-5A layer for three different boundary conditions. They exhibit rapid variations at the edges except when the edges are simply supported and electrically grounded. Further results at specific points are given in Table 5 for the three sets of boundary conditions.

7 Conclusions

We have extended the Eshelby-Stroh formalism to study the three-dimensional deformations of thick piezoelectric laminates subjected to arbitrary boundary conditions at the edges. The equations of static, linear, piezoelectricity are satisfied at every point of the body. The analytical solution is in terms of an infinite series; the boundary conditions and the continuity conditions at the interfaces between the laminae are used to determine the unknown

Table 5 Mechanical displacement, stresses, electric potential, and electric displacement at specific locations of a square [0 deg GE/90 deg GE/PZT-5A] laminate for various boundary conditions, $L_1/H=5$

Variable	SP-SP	CD-CD	FD-FD
$\tilde{u}_1(H)$	-1.933	-1.082	0.322
$\tilde{u}_3(H/2)$	14.325	10.851	35.728
$\tilde{\sigma}_{11}(H)$	9.329	6.652	6.991
$\tilde{\sigma}_{13}(0.8H)$	0.972	1.056	0.388
$\tilde{\sigma}_{23}(0.8H)$	0.384	0.096	1.216
$\tilde{\sigma}_{33}(H/2)$	0.419	0.462	0.356
$\tilde{\phi}(0.9H)$	-3.668	-3.020	-5.117
$\tilde{D}_3(H)$	21.563	13.301	29.818
$\tilde{u}_1(H)$	10.161	4.774	10.326
$\tilde{u}_3(H/2)$	-25.862	-14.205	-36.291
$\tilde{\sigma}_{11}(0)$	15.517	11.115	12.631
$\tilde{\sigma}_{13}(0.8H)$	1.042	0.057	1.389
$\tilde{\sigma}_{23}(0.8H)$	0.836	2.184	1.419
$\tilde{\sigma}_{33}(H/2)$	-0.119	-0.012	-0.112
$\tilde{\phi}(0.9H)$	0.505	0.502	0.506
$\tilde{D}_3(H)$	-9.878	-9.440	-10.000

coefficients. By keeping a large number of terms in the series solution, the mechanical displacements, stresses, electric potential, and electric displacement can be computed to any desired degree of accuracy.

We have computed results for a two-ply [0 deg PVDF/90 deg PVDF] laminate and a three ply [0 deg GE/90 deg GE/PZT-5A] hybrid laminate that is simply supported and electrically grounded on two opposite edges and subjected to various mechanical and electrical boundary conditions at the remaining two edges. The effect of either mechanically clamping the edges, simply supporting them or leaving them traction free and prescribing either the electric potential or the normal component of the electric displacement to vanish, has been delineated. It is observed that the solution, valid for thick plates, exhibits sharp variations near the edges except when they are simply supported and electrically grounded.

It is found that for the two-ply laminate, the total stored energy converges monotonically from above for the mechanical loading and from below for the electric loading. When the normal component of the electric displacement is prescribed to be zero at the edges, the longitudinal distribution of the component of the electric displacement in the thickness direction exhibits, near the edges, rapid variations in a region of width $0.1L$ where L equals the span of the square plate. However, the width of such a layer equals $0.02L$ for the longitudinal distribution of the transverse shear stress. For a sinusoidal loading on the top surface, the deflected shape of the midsurface is sinusoidal only when all four edges are simply supported. When the two opposite edges of the upper PZT layer are free but that of the lower one are clamped, most severe deformations occur at points on the interface where the free edge meets it.

For the three-ply hybrid laminate, the axial variation of the transverse shear stress on the midsurface of the PZT layer exhibits sharp variations in a region of width $0.1L$ near the clamped and traction free edges. The maximum value of the transverse shear stress occurs at a point on the interface between the PZT and the substrate when the edges are either simply supported or traction-free but at a point within the 0 deg graphite-epoxy lamina when the edges are clamped. The tabulated results presented herein should help establish the validity of various approximate theories. Finally we note that edge singularities, if any, have not been delineated by using special functions. The present technique seems to capture adequately the sharp variations in the fields near the clamped and traction-free edges but neither gives the order of the singularity nor its precise width. The interested reader should consult Ting [26]; Vel and Batra [27] have commented on this for a generalized plane-strain problem.

Acknowledgments

This work was partially supported by the NSF grant CMS9713453 and the ARO grant DAAG55-98-1-0030 to Virginia Polytechnic Institute and State University. R. C. Batra was also supported by an Alexander von Humboldt Award.

References

- [1] Crawley, E. F., and de Luis, J., 1987, "Use of Piezoelectric Actuators as Elements of Intelligent Structures," *AIAA J.*, **25**, pp. 1373–1385.
- [2] Im, S., and Atluri, S. N., 1989, "Effects of a Piezo-Actuator on a Finitely Deformed Beam Subjected to General Loading," *AIAA J.*, **27**, pp. 1801–1807.
- [3] Crawley, E. F., and Anderson, E. H., 1990, "Detailed Models of Piezoceramic Actuation of Beams," *J. Intell. Mater. Syst. Struct.*, **1**, pp. 4–25.
- [4] Lee, C. K., 1990, "Theory of Laminated Piezoelectric Plates for the Design of Distributed Sensors/Actuators. Part I: Governing Equations and Reciprocal Relationships," *J. Acoust. Soc. Am.*, **87**, pp. 1144–1158.
- [5] Wang, B. T., and Rogers, C. A., 1991, "Laminate Plate Theory for Spatially Distributed Induced Strain Actuators," *J. Compos. Mater.*, **25**, pp. 433–452.
- [6] Huang, J. H., and Wu, T. L., 1996, "Analysis of Hybrid Multilayered Piezoelectric Plates," *Int. J. Eng. Sci.*, **34**, pp. 171–181.
- [7] Mitchell, J. A., and Reddy, J. N., 1995, "A Refined Hybrid Plate Theory for Composite Laminates With Piezoelectric Laminae," *Int. J. Solids Struct.*, **32**, pp. 2345–2367.
- [8] Robbins, D. H., and Reddy, J. N., 1991, "Analysis of Piezoelectrically Actuated Beams Using a Layer-Wise Displacement Theory," *Comput. Struct.*, **41**, pp. 265–279.
- [9] Ha, S. K., Keilers, C., and Chang, F. K., 1992, "Finite Element Analysis of Composite Structures Containing Piezoceramic Sensors and Actuators," *AIAA J.*, **30**, pp. 772–780.
- [10] Heyliger, P., Ramirez, G., and Saravanos, D., 1994, "Coupled Discrete-Layer Finite Elements for Laminated Piezoelectric Plates," *Commun. Numer. Meth. Eng.*, **10**, pp. 971–981.
- [11] Batra, R. C., and Liang, X. Q., 1997, "Finite Dynamic Deformations of Smart Structures," *Comput. Mech.*, **20**, pp. 427–438.
- [12] Vlasov, B. F., 1957, "On One Case of Bending of Rectangular Thick Plates," *Vestnik Moskovskogo Universiteta. Seriya Matematika, mekhanika, astronomii, fiziki, khimii*, No. 2, pp. 25–34, (in Russian).
- [13] Pagano, N. J., 1969, "Exact Solutions for Composite Laminates in Cylindrical Bending," *J. Compos. Mater.*, **3**, pp. 398–411.
- [14] Pagano, N. J., 1970, "Exact Solutions for Rectangular Bidirectional Composites and Sandwich Plates," *J. Compos. Mater.*, **4**, pp. 20–34.
- [15] Srinivas, S., and Rao, A. K., 1970, "Bending, Vibration and Buckling of Simply Supported Thick Orthotropic Rectangular Plates and Laminates," *Int. J. Solids Struct.*, **6**, pp. 1463–1481.
- [16] Ray, M. C., Rao, K. M., and Samanta, B., 1993, "Exact Solution for Static Analysis of Intelligent Structures Under Cylindrical Bending," *Comput. Struct.*, **47**, pp. 1031–1042.
- [17] Heyliger, P., and Brooks, S., 1996, "Exact Solutions for Laminated Piezoelectric Plates in Cylindrical Bending," *ASME J. Appl. Mech.*, **63**, pp. 903–910.
- [18] Bisegna, P., and Maceri, F., 1996, "An Exact Three-Dimensional Solution for Simply Supported Rectangular Piezoelectric Plates," *ASME J. Appl. Mech.*, **63**, pp. 628–638.
- [19] Lee, J. S., and Jiang, L. Z., 1996, "Exact Electroelastic Analysis of Piezoelectric Laminae via State Space Approach," *Int. J. Solids Struct.*, **33**, pp. 977–990.
- [20] Heyliger, P., 1994, "Static Behavior of Laminated Elastic/Piezoelectric Plates," *AIAA J.*, **32**, pp. 2481–2484.
- [21] Heyliger, P., 1997, "Exact Solutions for Simply Supported Laminated Piezoelectric Plates," *ASME J. Appl. Mech.*, **64**, pp. 299–306.
- [22] Tang, Y. Y., Noor, A. K., and Xu, K., 1996, "Assessment of Computational Models for Thermoelastic Multilayered Plates," *Comput. Struct.*, **61**, pp. 915–933.
- [23] Saravanos, D. A., Heyliger, P. R., and Hopkins, D. A., 1997, "Layerwise Mechanics and Finite Element for the Dynamic Analysis of Piezoelectric Composite Plates," *Int. J. Solids Struct.*, **34**, pp. 359–378.
- [24] Eshelby, J. D., Read, W. T., and Shockley, W., 1953, "Anisotropic Elasticity With Applications to Dislocation Theory," *Acta Metall.*, **1**, pp. 251–259.
- [25] Stroh, A. N., 1958, "Dislocations and Cracks in Anisotropic Elasticity," *Philos. Mag.*, **3**, pp. 625–646.
- [26] Ting, T. C. T., 1996, *Anisotropic Elasticity. Theory and Applications*, Oxford University Press, New York.
- [27] Vel, S. S., and Batra, R. C., 2000, "The Generalized Plane Strain Deformations of Thick Anisotropic Composite Laminated Plates," *Int. J. Solids Struct.*, **37**, pp. 715–733.
- [28] Vel, S. S., and Batra, R. C., 2000, "Cylindrical Bending of Laminated Plates With Distributed and Segmented Piezoelectric Actuators/Sensors," *AIAA J.*, **38**, pp. 857–867.
- [29] Vel, S. S., and Batra, R. C., 1999, "Analytical Solution for Rectangular Thick Laminated Plates Subjected to Arbitrary Boundary Conditions," *AIAA J.*, **37**, pp. 1464–1473.
- [30] Tiersten, H. F., 1969, *Linear Piezoelectric Plate Vibrations*, Plenum Press, New York.
- [31] Suo, Z., Kuo, C.-M., Barnett, D. M., and Willis, J. R., 1992, "Fracture Mechanics for Piezoelectric Ceramics," *J. Mech. Phys. Solids*, **40**, pp. 739–765.
- [32] Tashiro, K., Tadokoro, H., and Kobayashi, M., 1981, "Structure and Piezoelectricity of Poly(Vinylidene Fluoride)," *Ferroelectrics*, **32**, pp. 167–175.
- [33] Nye, J. F., 1985, *Physical Properties of Crystals*, Oxford University Press, New York.
- [34] Batra, R. C., Liang, X. Q., and Yang, J. S., 1996, "The Vibration of a Simply Supported Rectangular Elastic Plate Due to Piezoelectric Actuators," *Int. J. Solids Struct.*, **33**, pp. 1597–1618.